Journal of Basic Physical Research ISSN: 2141-8403 Prints, 2141-8411 Online
Vol.14, Issue 2, October, 2025, pp. 79 – 99, Available online at https://journals.unizik.edu.ng/jbpr/

CASSON FLUID FLOW IN A VERTICAL CHANNEL INCORPORATING SUCTION, HEAT SINK AND DUFOUR MECHANISMS

Farisa Muhammad[1], Emmanuel Omokhuale[1], Salisu Muhammad Muhammad[1] and Lawal Sa'adu[2]
[1]Department of Mathematical Sciences, Federal University Gusau, P. M. B. 1001, Zamfara State, Nigeria.
[2]Department of Physics, Federal University Gusau, P. M. B. 1001, Zamfara State, Nigeria.
Corresponding Author's ***Email: farisamuhammad02@gmail.com***

Abstract
In this paper, we have investigated Casson fluid Flow in a vertical channel incorporating suction, heat sink and Dufour mechanisms. The governing equations are modeled using Casson model by considering Dufour and heat sink. The equations are non-dimensionalised by defining suitable dimensionalising parameters. The resulting equations are nonlinear and coupled. These are tackled by employing regular perturbation technique. Velocity, temperature and concentration are plotted for various physical parameters which affects the flow and are analysed graphically. The method is observed to give good agreement. It is seen that increase in Dufour and heat sink parameters lead to rise in both thermal and momentum boundary layers.
Keywords: *MHD; Casson fluid; Dufour; heat sink and channel flow.*

Nomenclature

List of variable

Gc	Thermal Grashof Number
Gm	Mass Grashof Number
Pr	Prandtl Number
Rc	Chemical Reaction Parameter
M	Magnetic Parameter
S	Suction parameter
K	Permeability parameter
Sc	Schmidt Number
Du	Dufour number (Diffusion Thermo)
T^*	Temperature of fluid (K)
T_w^*	Temperature of fluid near to moving plate (K)
T_0^*	Temperature of fluid near to stationary plate (K)
C^*	Concentration of fluid (mol m^{-3})
C_w^*	Concentration of fluid near to moving plate (mol m^{-3})
C_0^*	Concentration of fluid near to the stationary plate (mol m^{-3})
t^*	Time in x^*, y^* coordinate system (s)
u_0	Reference velocity (ms^{-1})
C_p	Specific heat at constant pressure $(JKg^{-1}K)$
D_c	Mass diffusivity (m^2s^{-1})
T_m	Mean fluid temperature (K)
k_T	Thermal diffusion ratio
k_c	Mean absorption coefficient

g Acceleration due to gravity (ms^{-1})
Q_0 The heat generation constant
y^* Dimensional coordinate perpendicular to the plate
C^* Dimensional concentration of the fluid
T^* Dimensional temperature of the fluid
u^* Dimensional velocity of the fluid
U Dimensionless velocity of the fluid
t Dimensionless time
h Distance between two parallel plate
Q_r Heat absorption flux
k_p Thermal conductivity (W $K^{-1}m^{-1}$)

Greek symbols

β Casson Parameter
β_1 Volumetric coefficient of thermal expansion
β_2 Volumetric coefficient of concentration
ρ Fluid Density
υ Kinematic Viscosity
φ_1 Heat Absorption Parameter
σ Electric Conductivity of the Fluid (ms^{-1})
ε Activation energy parameter
η Dimensionless coordinate perpendicular to the plate
λ Dimensionless concentration of the fluid
ξ Dimensionless temperature of the fluid

Subscripts

0 Condition in the free stream
P Plate
w Wall condition

Superscript

* Dimensional

Introduction

The study of Casson fluid flow in a channel, incorporating constant suction, a heat sink, and Dufour mechanisms, investigates the behavior of a non-Newtonian fluid with a yield stress and shear-thinning properties in a controlled flow environment. The inclusion of constant suction introduces a force that draws the fluid towards the channel walls, while the heat sink simulates a cooling effect and the Dufour mechanism, also known as thermos-diffusion, involves the effect of heat gradients on the diffusion of fluid components. This analysis is relevant for understanding the flow and heat transfer characteristics of Casson fluids in various engineering applications, such as blood flow, polymer processing, and other systems where non-Newtonian behavior is significant.

The term "Casson fluid" describes a type of non-Newtonian fluid characterized by variable viscosity. The dominance of viscous force in this system can be attributed to the action of variable viscosity in the fluid. Fluids commonly employed in many applications include paints, diverse polymer solutions, blood, honey, etc. Typical instances of Casson fluids encompass synthetic lubricants, mud extraction, clay coatings, and biomedical fluids. The Casson fluid

simulations that are readily accessible are classified based on their distinct rheological properties, including Oldroyd-B, Eyring-Powell, Oldroyd-A, Maxwell, Carreau, Jeffrey, and Burger. In the field of modern technology, there are some flow features that defy comprehension when analyzed solely through the lens of the Newtonian flow model (Ojemeri *et al*., 2025). The Casson fluid model has found applications in various fields such as: food science (e.g., describing ketchup, toothpaste), biomedical engineering (e.g., blood flow in arteries), and industrial processes (e.g., paints, drilling fluids). Researchers have developed extensions and modifications of the Casson model to better fit specific types of fluids or to incorporate additional complexities (Kumar and Singh, 2023).

Casson fluid model was initially proposed by Casson in 1959 for the anticipation of flow trends of suspended pigment-oil1. In the case of small shear stress, Casson fluid behaves like an elastic solid and no flow takes place. On the other hand, the dominance of the shear stress magnitude of Casson fluid against yield shear stress ensures the flow of Casson fluid. This fluid is based on a structural model of bilateral behavior of liquid and solid phases of two-phase suspension. Some significant examples of Casson fluid are honey, jelly, soup, concentrated fruit juices, and artificial fibers. The participation of Casson fluid can be observed in the preparation of multiple products such as synthetic lubricants, pharmaceutical chemicals, paints, coal, tomato sauce, china clay, and many others. Since human blood is comprised of various substances like fibrinogen, human red blood cells, protein, and globulin in aqueous base plasma, it can also be considered as Casson fluid. A wide variety of researchers have been fascinated by efficacious applications of Casson fluid in drilling processes, biological treatments, food processing, and bio-engineering operations (Anwar *et al*. 2021). Anwar *et al*. (2021) discussed on unsteady magnetohydrodynamic flow of Casson fluid over an infinite vertical plate is examined under ramped temperature and velocity conditions at the wall. Thermal radiation flux and heat injection/ suction terms are also incorporated in the energy equation. The electrically conducting fluid is flowing through a porous material and these phenomena are governed by partial differential equations. After employing some adequate dimensionless variables, the solutions are evaluated by dint of Laplace transform.

Vertical channels are commonly found in various thermal engineering equipment, such as solar energy collectors and cooling devices for electronic and micro-electronic equipment. Given their extensive use, numerous studies have been conducted to explore the characteristics of fully developed mixed convection flow in these vertical channels. Due to its wide applications, a lot of investigations have been done toward the understanding of fully developed mixed convection flow in a vertical channel (Xu and Pop, 2012; Nur *et al*. (2024). Grosan and Pop (2007) analyzed the influence of thermal radiation on steady, fully developed mixed convection in vertical channels. They examined cases where the channel walls have uniform but different wall temperatures using the Rosseland approximation model. This model resulted in ordinary differential equations for an optically dense viscous incompressible fluid flowing through the channel.

Israel-Cookey *et al*. (2023) investigated magnetohydrodynamic forced convection and heat transfer of a Casson fluid flow in an anisotropic porous channel with isoflux boundaries. Ramesh *et al*. (2023) examined the impact of diffusion-thermal effects on mixed convective Casson fluid flow through a permeable channel. Their study focused on laminar flow regimes and does not extend its analysis to turbulent flow conditions, which are common in industrial applications. Dinesh *et al*. (2023) studied the Soret impact on mixed convection of Casson fluid flow in the occurrence of porous media within a permeable channel. The model does not

account for the variation in porosity or permeability of the medium, which could significantly affect the flow behavior in practical situations.

The manipulation of suction and injection holds significance in regulating fluid dynamics, making it a crucial factor in addressing practical challenges related to film cooling and controlling boundary layers. This applies across various fields such as industrial, geophysical, biomedical, engineering, and environmental applications (Ismail *et al*. 2025).

Heat sources and sinks refer to regions where heat is added to or removed from a system. They play a critical role in thermal management in engineering systems. In many practical scenarios, such as heat exchangers, reactors, and thermal insulation systems, managing heat transfer through fluids is vital for optimizing performance and safety. The inclusion of heat sources or sinks in fluid dynamics research is essential for applications such as geothermal energy extraction, chemical reactors, and biological systems. Heat transfer models must account for these sources to predict temperature distributions accurately and optimize performance. An internal heat source is a process that generates heat within a material or system. This can be due to a variety of sources, including chemical reactions, nuclear reactions, or electrical resistance (Vinod *et al.,* 2024a). Several authors has investigated on heat source and sink, such as Ojemeri and Hamza (2022) presented a theoretical investigation of a chemically reactive fluid in a MHD natural convection flow blended with heat source and sink effects employing homotopy perturbation approach. They concluded that raising the viscous heating parameter significantly encourage the fluid motion and the volume flow rate respectively. Oni and Jha (2019) investigated the effects of a heat source and sink fluid on natural convection confined to an upstanding annulus with time-periodic heating boundary conditions. They discovered that heat generation and absorption parameters affect velocity distribution, periodic temperature profile, Nusselt number, and frictional force at the cylinder walls, respectively.

The Dufour effect describes the temperature caused by concentration gradients, while the Soret outcome refers to the concentration caused by temperature gradients (Vinod *et al.,* 2024a). Furthermore, the energy flux caused by a composition gradient is called diffusion-thermo or Dufour effect. Diffusion-thermal effect can also be found in the energy equation. Generally, Dufour effect is of smaller order of magnitude than the effects prescribed by Fourier and Fick's laws. However, it is mostly neglected by many authors in the investigation of heat and mass transfer (Falodun and Ahamed, 2019). the Dufour effect on unsteady free convection flow in a vertical channel under the influence of inclined magnetic field, heat generation or absorption and the first-order chemical reaction has not been addressed in the literature even though this problem finds potential applications in the chemical processing equipment, geothermal energy systems, cooling of nuclear reactors and in the design of heat exchangers. It seems that there is no much information available on Dufour effect as compared to the Soret effect for double-diffusive natural convection flows (Qiang, *et al*., 2020). Babu *et al*. (2018) explained how the Soret and Dufour effects affect mass and heat transfer in chemically reacting MHD flow via a wavy channel. A study conducted by Uwanta and Hamza (2014) investigated the influence of the Soret and Dufour effects on the flow of free convective heat and mass transfer in a channel with constant suction and viscous dissipation. Sharma and Bhaskar (2020) studied the impact of heat radiation and chemical reactions on three-dimensional magnetohydrodynamic (MHD) incompressible and viscous flows, taking into account the Dufour and Soret effects. Gbadeyan *et al*. (2018) analyzed the influence of Dufour and Soret phenomena on chemically reacting MHD flow through a wavy channel, specifically looking at the impacts of Dufour on mass and heat transfer. Unsteady MHD Flow of Viscoelastic Micropolar Fluid Past an Infinite Vertical Plate with a Heat Source.

Most recently, Vinod et al. (2024b) researched on Dufour and Soret effects on double diffusive Casson fluid flow with the influence of internal heat source. Prakash *et al*. (2025) focused on thermal and radiative effects on unsteady MHD flow of Casson fluid past a rotating porous medium with variable mass diffusion. Kumar *et al*. (2025) showed the impacts of thermos-diffusion on unsteady MHD free convection mass and heat flow past an accelerating vertical porous plate in the existence of radiation. This analysis is carried out by numerically solving the dimensionless equations by the use of the finite difference approach (FDM). Shankar & Sheri (2025) investigated the impact of Dufour effects and viscous dissipation on unsteady magnetohydrodynamic (MHD) natural convection in an incompressible, viscous, and electrically conductive fluid over a vertically oscillating flat plate. Their study highlighted the significance of magnetic fields in influencing thermal and mass transfer, particularly in the context of thermal radiation.

The above referenced works and their abundant potential applications motivated us to conduct the current analytical investigation to examine the influence of Dufour effect on Casson fluid flow in a vertical channel, as this problem has not been discussed in the literature yet. The Dufour effect is induced by the heat flux generated and they are a key factor in the issues associated with the movement of contaminants in groundwater and the use of geothermal reservoirs. Other important industrial uses include: cooling towers, sorption at an interface (adsorption) or in a bulk, drying and humidifying, segregation and doping in materials, vaporization and condensation in a mixture, boiling at a solid surface, combustion, and most other chemical reactions (absorption).

Casson Fluid Model

The Casson fluid model is a rheological model commonly used to describe non-Newtonian fluids, particularly those that exhibit a yield stress. This model was initially developed to describe the flow of materials like: blood and chocolate, which do not flow until a certain threshold (yield tress) is exceeded. The rheological equation or state of Cauchy stress tensor of Casson fluid is written as

$\tau=\tau_0+\mu\dot{\gamma}$

or

$$\tau_{ij}=\begin{cases}2\left(\mu_\beta+\frac{P_y}{\sqrt{2\pi}}\right)e_{ij}, & \pi>\pi_c\\ 2\left(\mu_\beta+\frac{P_y}{\sqrt{2\pi}}\right)e_{ij}, & \pi>\pi_c\end{cases}$$

where $\pi= e_{ij}$ and e_{ij} is the $(i,j)^{th}$ component of the deformation rate, π is the product of the component of deformation rate with itself. Also, π_c is a critical value of this product based on the non-Newtonian model, μ_β is plastic dynamic viscosity of the non-Newtonian fluid and P_y is yield stress fluid.

Mathematical Formulation of the Problem

Consider the case of a Casson fluid stream that is moving through a porous medium while passing through a vertical channel. On an electrically conducting fluid that is perpendicular to the channel, a consistent magnetic field of strength B_0 is applied.

To ensure controllability and to simplify the problem, several assumptions and approximations were made during the modelling process:

1. It is assumed that the fluid exhibits non-Newtonian behavior, where the relationship between shear stress and shear rate is nonlinear.
2. It is assumed that the fluid is incompressible, with a constant density and free convective.
3. We assume that the material properties, such as viscosity, thermal conductivity, and specific heat, are constant throughout the flow field.
4. We further assume that the effects of Dufour and heat sink are not negligible.

In accordance with the aforementioned assumptions and taking into account Boussinesq's approximation, the partial differential equations that govern the situation with initial and boundary conditions is as follows:

$$\frac{\partial v}{\partial y} = 0 \tag{1}$$

$$\rho\left[\frac{\partial u^*}{\partial t^*} + v\frac{\partial u^*}{\partial y^*}\right] = \mu\left(1+\frac{1}{\beta}\right)\frac{\partial^2 u^*}{\partial y^{*2}} - \delta\beta_0^2 u^* + \rho g\beta_1\left(T^* - T_h^*\right) + \rho g\beta_2\left(C^* - C_h^*\right) - \left(1+\frac{1}{\beta}\right)\frac{\mu\varphi}{K_p}u^* \tag{2}$$

$$\rho C_p\left[\frac{\partial T^*}{\partial t^*} + v\frac{\partial T^*}{\partial y^*}\right] = K_T\frac{\partial^2 T^*}{\partial y^{*2}} - Q_0\left(T^* - T_h^*\right) + \frac{D_c K_T}{T_m}\frac{\partial C^*}{\partial y^{*2}} \tag{3}$$

$$\frac{\partial C^*}{\partial t^*} + v\frac{\partial C^*}{\partial y^*} = Dc\frac{\partial^2 C^*}{\partial y^{*2}} - Kc\left(C^* - C_h^*\right) \tag{4}$$

The initial and boundary conditions for these equations are assumed as follows:

$$t^* \le 0 : u^* = 0, \xi^* = T_\infty^*, \lambda^* = C_\infty^* \text{ for all } y^*$$

$$t^* > 0\begin{cases} u^* = 0, \xi^* = T_h^* + \left(T_w^* - T_h^*\right)\grave{o}e^{iwt}, \lambda^* = C_h^* + \left(C_w^* - C_h^*\right)\grave{o}e^{iwt} \text{ at } y^* = 0 \\ u^* \to 0, \xi^* \to T_h^*, \lambda^* \to C_h^* \quad as\ y^* \to \infty \end{cases} \tag{5}$$

Solving (1), $\frac{\partial v}{\partial y} = 0 \Rightarrow v^* = -v_0$ (6)

We define the following dimensionless quantities

$$\eta = \frac{y^*}{h}, u = u^* u_0, t = \frac{t^*\upsilon}{h^2}, \xi = \frac{T^* - T_0^*}{qh}, \lambda = \frac{C^* - C_\infty^*}{qh} \tag{7}$$

Substituting (6) and (7) into equations (2), (3) and (4), then we have the following dimensionless form of the equations:

$$\frac{\partial u}{\partial t} - S\frac{\partial u}{\partial \eta} = \left(1+\frac{1}{\beta}\right)\frac{\partial^2 u}{\partial \eta^2} - \left(M + \left(1+\frac{1}{\beta}\right)\frac{1}{K}\right)u + Gr\xi + Gm\lambda \tag{8}$$

$$\frac{\partial \xi}{\partial t} - S\frac{\partial \xi}{\partial \eta} = \frac{1}{\Pr}\frac{\partial^2 \xi}{\partial \eta^2} + \varphi_1\xi + Du\frac{\partial^2 \lambda}{\partial \eta^2} \tag{9}$$

$$\frac{\partial \lambda}{\partial t} - S\frac{\partial \lambda}{\partial \eta} = \frac{1}{Sc}\frac{\partial^2 \lambda}{\partial \eta^2} - Rc\lambda \tag{10}$$

where $Sc = \frac{\upsilon}{D_c}, M = \frac{\sigma\beta_0^2 h^2}{\rho\upsilon}, Gr = \frac{u_0 h^3 qg\beta_1}{\upsilon}, Gm = \frac{u_0 h^3 qg\beta_2}{\upsilon}, Rc = \frac{k_c h^2}{\upsilon},$

$S = \frac{v_0 h}{\upsilon}, K = \frac{k_p}{h^2\varphi}, Du = \frac{D_c k_T}{T_m c_p \mu}, \varphi_1 = \frac{Q_0 h^2}{\mu c_p}, \Pr = \frac{\mu c_p}{K_T},$

The corresponding initial and boundary conditions in dimensionless form become:

$u = 0, \xi = 1 + \varepsilon e^{iwt}, \lambda = 1 + \varepsilon e^{iwt}, at\ \eta = 0$

$u = 0, \xi = 1, \lambda = 1, at\ \ \eta \to 0$

$u = 0, \xi = 0, \lambda = 0, at\ \ \eta = 1$ (11)

ANALYTICAL SOLUTIONS

Equations (8) to (10) represent the dimensionless governing equations along with initial and boundary conditions (11), which describe the behavior of the system in study. In order to obtain analytical solutions, the regular perturbation method is employed. We assume solutions of the form:

$u(\xi,\tau) = u_0(\xi) + u_1(\xi)\varepsilon e^{iwt}$ (12)

$\xi(\xi,\tau) = \xi_0(\xi) + \xi_1(\xi)\varepsilon e^{iwt}$ (13)

$\lambda(\xi,\tau) = \lambda_0(\xi) + \lambda_1(\xi)\varepsilon e^{iwt}$ (15)

The following are set of ODEs are derived:

$u_0 : u_0^{"} + \frac{S}{\gamma}u_0^{'} - \phi u_0 = -\frac{Gr}{\gamma}\xi_0 - \frac{Gm}{\gamma}\lambda_0$ (16)

$u_1 : u_1^{"} + \frac{S}{\gamma}u_1^{'} - \left(\frac{iw}{\gamma} + \phi\right)u_1 = -\frac{Gr}{\gamma}\xi_1 - \frac{Gm}{\gamma}\lambda_1$ (17)

$\xi_0 : \xi_0^{"} + \Pr S\xi_0^{'} + \Pr\varphi_1\xi_0 = -\Pr Du\lambda_0^{"}$ (18)

$\xi_1 : \xi_1^{"} + \Pr S\xi_1^{'} + (\Pr\varphi_1 - iw\Pr)\xi_1 = -\Pr Du\lambda_1^{"}$ (19)

$\lambda_0 : \lambda_0^{"} + ScS\lambda_0^{'} - ScKc\lambda_0 = 0$ (20)

$\lambda_1 : \lambda_1^{"} + ScS\lambda_1^{'} - (iwSc + ScKc)\lambda_1 = 0$ (21)

Subject to the following boundary condition:

$u_0 = u_1 = 0, \xi_0 = \xi_1 = 1, \lambda_0 = \lambda_1 = 1 \text{at}\ \eta = 0$

$u_0 = u_1 = 0, \xi_0 = \xi_1 = 0, \lambda_0 = \lambda_1 = 0\ \text{at}\ \eta = 1$ (22)

As a result, the received solutions are the solutions of the described problem under the given initial and boundary conditions. This approach yields the final analytical solutions for the fluid's velocity, temperature and concentration are as follows, respectively:

$$u(\eta,t) = A_{13}e^{n_9\eta} + A_{14}e^{-n_{10}\eta} + A_{15}e^{n_5\eta} + A_{16}e^{-n_6\eta} + A_{17}e^{n_1\eta} + A_{18}e^{-n_2\eta} + A_{19}e^{n_1\eta} + A_{20}e^{-n_2\eta} + (A_{21}e^{n_{11}\eta} + A_{22}e^{-n_{12}\eta} + A_{23}e^{n_7\eta} + A_{24}e^{-n_8\eta} + A_{25}e^{n_3\eta} + A_{26}e^{-n_4\eta} + A_{27}e^{n_3\eta} + A_{28}e^{-n_4\eta})\varepsilon e^{iwt}$$ (23)

$$\xi(\eta,t) = A_5e^{n_5\eta} + A_6e^{-n_6\eta} + A_7e^{n_1\eta} + A_8e^{-n_2\eta} + (A_9e^{n_7\eta} + A_{10}e^{-n_8\eta} + A_{11}e^{n_3\eta} + A_{12}e^{-n_4\eta})\varepsilon e^{iwt}$$ (24)

$$\lambda(\eta,t) = A_1 e^{n_1\eta} + A_2 e^{-n_{25}\eta} + (A_3 e^{n_3\eta} + A_4 e^{-n_4\eta})\varepsilon e^{iwt} \quad (25)$$

The Skin-friction, rate of heat and mass transfer, respectively at wall are as follows:

$$C_f = -\left(\frac{dU}{d\eta}\right)_{\eta=0} = n_9 A_{13} - n_{10} A_{14} + n_5 A_{15} - n_6 A_{16} + n_1 A_{17} - n_2 A_{18} + n_1 A_{19} - n_2 A_{20} + (n_{11} A_{21} - n_{12} A_{22} + n_7 A_{23} - n_8 A_{24} + n_3 A_{25} - n_4 A_{26} + n_3 A_{27} - n_4 A_{28})\varepsilon e^{iwt} \quad (26)$$

$$Nu = -\left(\frac{d\xi}{d\eta}\right)_{\eta=0} = n_5 A_5 - n_6 A_6 + n_1 A_7 - n_2 A_8 + (n_7 A_9 - n_8 A_{10} + n_3 A_{11} - n_4 A_{12})\varepsilon e^{iwt} \quad (27)$$

$$Sh = -\left(\frac{d\lambda}{d\eta}\right)_{\eta=0} = n_1 A_1 - n_2 A_2 + (n_3 A_3 - n_4 A_4)\varepsilon e^{iwt} \quad (28)$$

RESULTS AND DISCUSSION

In this section, we present a detailed analysis of the Dufour and heat sink effects within the MHD flow of Casson fluid in a porous channel performed with MATLAB. Through variation of parameters like: Casson fluid, magnetic, porosity, heat source parameters and mass Grashof, thermal Grashof, Dufour, Schmidt, Prandtl numbers, the effect of each factor on the velocity, temperature and concentration profiles is assessed. The graphical results demonstrate the effect of these parameters on the momentum, thermal and concentration boundary layers and show some notable patterns or trends. Such insights of the behavior of the fluid under different conditions is crucial in order to tailor such systems for MHD flow systems in engineering applications.

Illustration for Velocity Profile

In Figure 1, the effect of Prandtl number on velocity profiles. It is observed that the velocity decreases as Prandtl number becomes significant. Figure 2 depicts the effect of Dufour number on the momentum boundary layer. It is observed that the velocity of the fluid rises as Dufour parameter is increased. Effect of heat sink on the velocity of the fluid is shown in Figure 3, it is clear that the velocity is higher due to an increase in the heat sink parameter. In Figure 4, the effect of chemical reaction on the momentum boundary layer is presented, it is found that increase in the chemical reaction parameter causes the velocity of the fluid to reduce. Figure 5 connotes the effect of Schmidt number on the velocity of the fluid, it is observed that the fluid's velocity reduces as Schmidt number become significant. The effect of suction on the velocity profile is shown in Figure 6, it is noticed that increase in suction parameter leads to a fall of the velocity of the fluid. The outcome of this study concerning effects of mass Grashof number are illustrated on Figure. It is observed that not only the temperature gradients in the thermal Grashof number foster convection motion but concentration gradients in the mass Grashof number increase the fluid motion which brings about a more complex velocity profile. As we move on stress, the mass Grashof number indicates that the denser fluid due to concentration gradients generates stronger buoyancy forces that cause thermal convection and aid movement of fluids within the higher concentration zones compared to lower concentration zones. Therefore, the velocity profile is enhanced with an increase in mass Grashof number, as the concentration gradient buoyant force enhances the movement of the fluid. Figure 8 showcases the effect of thermal Grashof number on the changes in the velocity profiles. It is noticed that the velocity profile rises considerably. As seen, the increase in the thermal Grashof number indicates an increase in the temperature difference between the fluid layers and this causes an increase in buoyant forces to act in the warmer regions of the fluid and thus assists in movement. Therefore, as thermal Grashof number values are consistently higher, it is expected that the velocity profile shows a greater since more fluid is pushed, creating an

increase in flow because of buoyant forces. This has an even greater effect in natural convection where diversion forces such as: pumps, or fans are absent. In the case where the fluid is close to the heated surface., the elevation of thermal Grashof number certainly cause a rise in the velocity at the boundary because the less dense hot fluid rises and the much denser cold fluid moves down to occupy space. This explains how a more steep velocity profile development can be observed as was shown in velocity profile analysis. The Lorentz force depends on the magnetic parameter and since it constitutes the velocity profile, it is dependent on the strength of the magnetic field as well. In Figure 9, it can be seen that the increase in magnetic field strength leads to remarkable slowdown of the magnetic parameter velocity profile. The magnetic Lorentz force acts normal to both the fluid motion and the magnetic field causing resistive forces acting against the movement of numerous particles in the fluid. The role of the bent Lorentz force is to serve as a damping mechanism of the shear stress which of course will eventually lead to the reduction of the fluid flow. This resistance leads to the decrease of velocity where higher magnetic velocities could be seen to be reduced instead. As the strength of the magnetic field increases the depleting motion increases and as a result, the fluid motion reduces. The electrically conducting fluid moves in the presence of magnetic field. Due to such a fluid a race of charged particles are formed as a result particles experience a force due to the movement of particles which retards it. This has a drag type effect, making even more the fluid slower. This behavior can be considered as fundamental in applications that involve magnetic fields for the purpose of controlling the motion of the fluid by limiting its free motion. Therefore, due to an increase of the magnetic parameter, the velocity profile is significantly reduced, and it perfectly exemplifies the effect of magnetic field on the motion of the fluid.

In Figure 10, the relation between the Casson parameter and the velocity profile, and more specifically its effect on the boundary layer has been depicted. However, since the Casson parameter increases, the amount of shear that the fluid can withstand increases as well. In the beginning, one could anticipate that the increase in resistance would reduce the velocity of the fluid close to the boundary of the layer and the reason being the fluid's high resistance to the applying shear forces. However, when the Casson parameter is increased, even the yield stress of the fluid goes up which allows the fluid to withstand more deformation before yield, thereby increasing the value of stress. Such yields stress compensation effects make it possible for the apparent wall shear stress to be larger. This results in lower induced velocity being developed along with a reduction in the angle with which higher Casson parameters become capable in developing suspensions. So, the Casson parameters have an inverse relation in the stability limit while showing more enhancement in the amount flow angle. From this, we reach a very important conclusion: with an increase of the Casson parameter the velocity increases along with the increase of the yield stress which comes in handy to counteract the resistance to the flow. When the porosity parameter is increased, the inherent drag forces between the fluid and the solid particles of the medium is decreased, which directly facilitates better movement of the fluid allowing for a more robust and sharper velocity profile. Porous and permeable mediums have a more free flowing motion due to the less drag they have to experience, which helps reduce resistance. It is vital to mention that though the fluid has to exert some force against the solid particles of the medium, the interaction is greatly reduced and the permeability is improved. When the porosity parameter is increased, the permeability is enhanced and the medium in question offers even less resistance to the fluid. Hence due to the already reduced drag, when the fluid is forced to interact with the solid matrix in a porous structure, the medium permeability increases, leading to a faster flow and higher movement rate of the fluid, as shown in Figure 11. As a result, an increase in porosity allows the fluid to meet less resistance and subsequently obtain a higher velocity profile. The impact is

considerable for filtration systems, soils, or other porous materials systems because increasing the porosity permits for less fluid transport obstruction and thus more rapid velocity profiles. Therefore, a favorable flow through the increase in the porosity parameter is beneficial because the fluid meets less resistance within the medium which results in a more profound as well as a higher velocity profile.

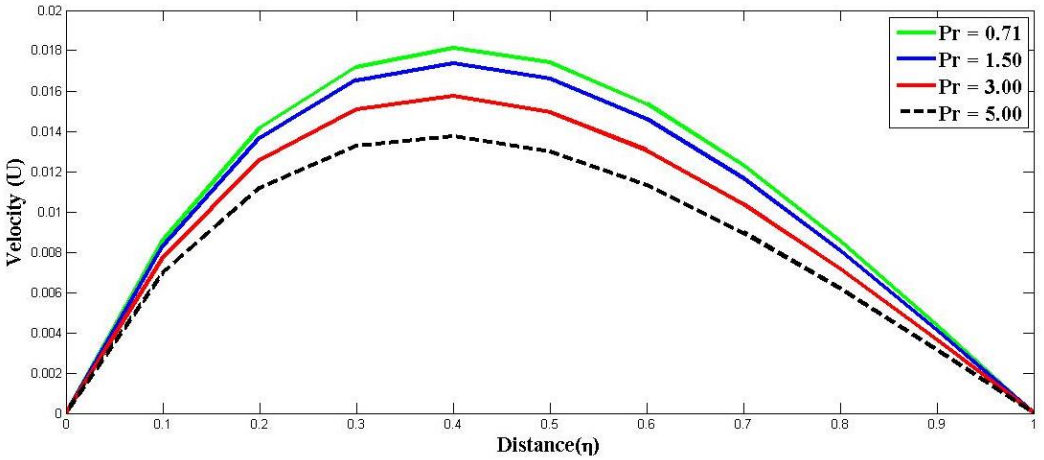

Figure 1: Velocity profile variations for Pr.

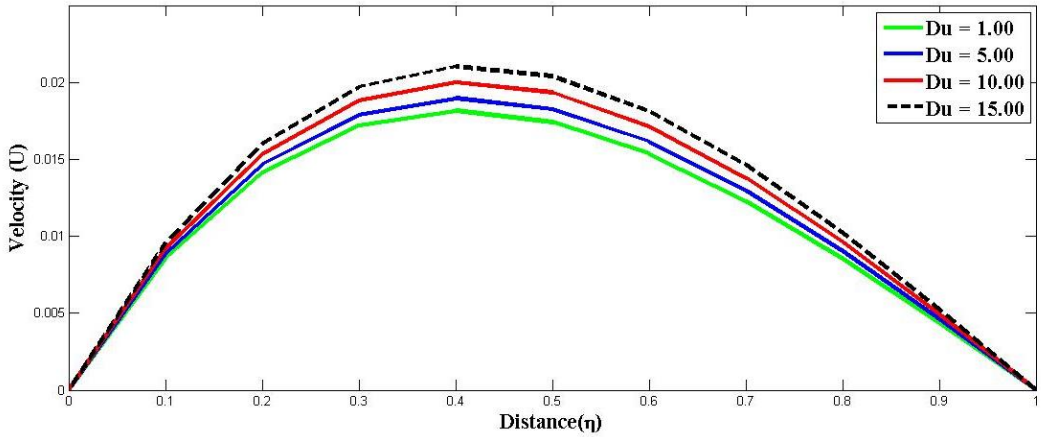

Figure 2: Velocity profile variations for Du.

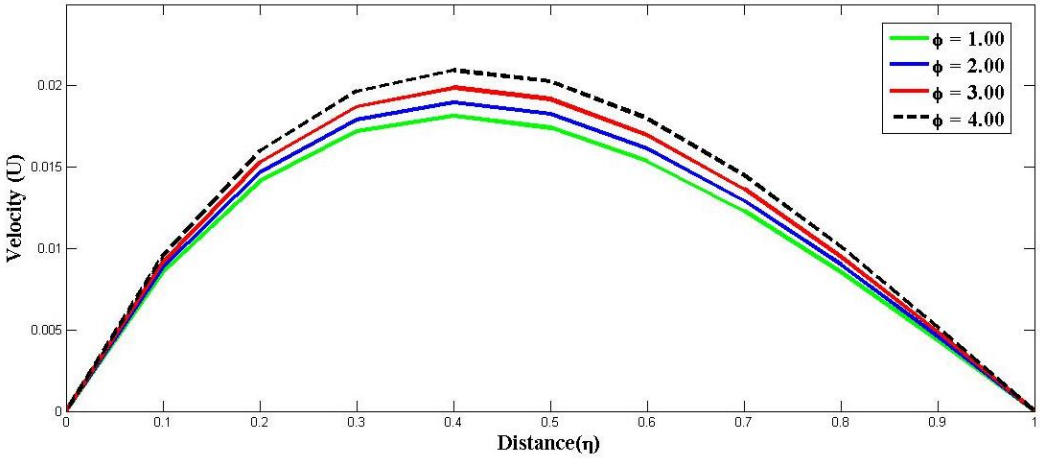

Figure 3: Velocity profile variations for φ_1.

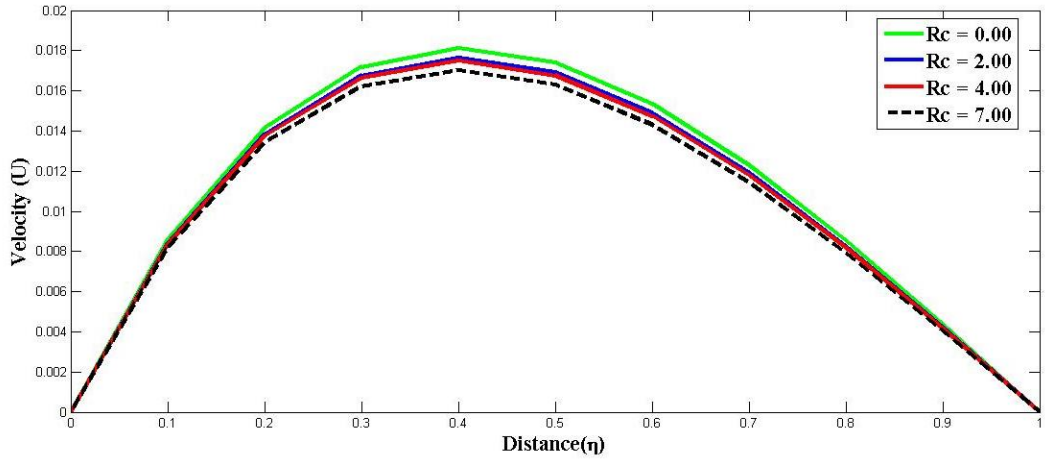

Figure 4: Velocity profile variations for Rc.

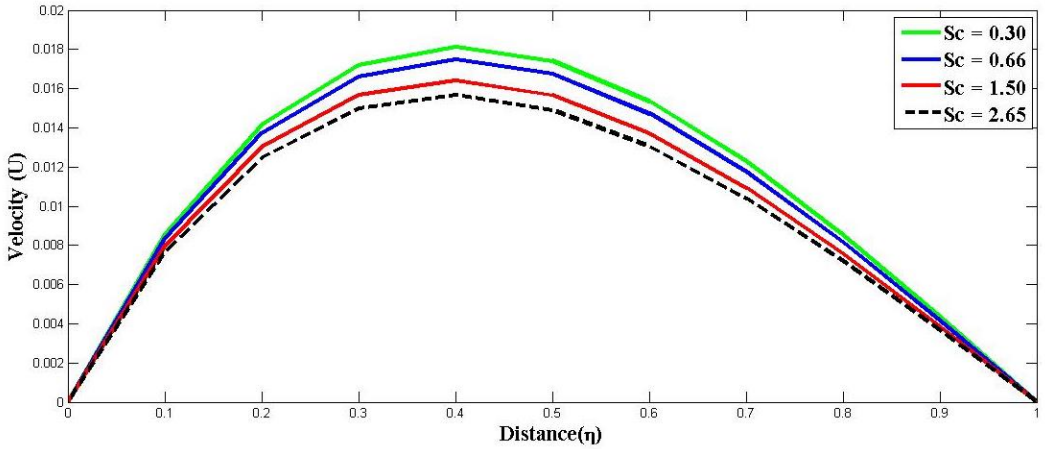

Figure 5: Velocity profile variations for Sc.

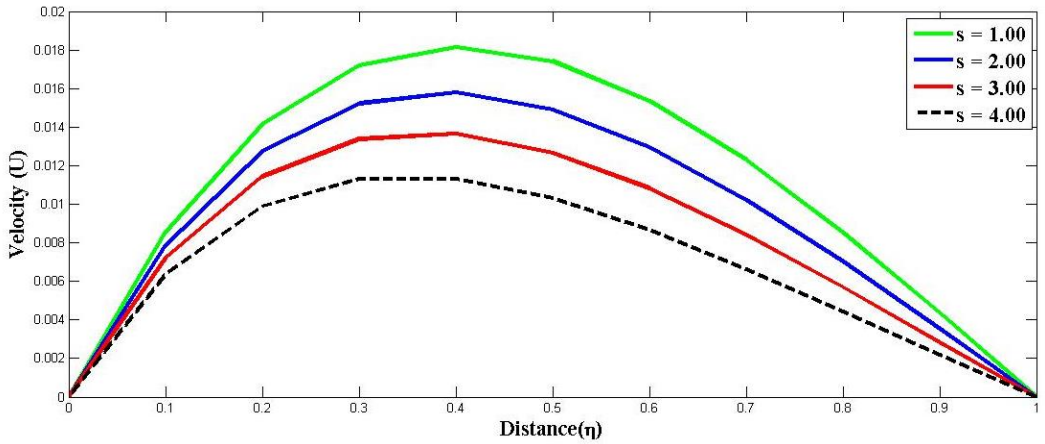

Figure 6: Velocity profile variations for s.

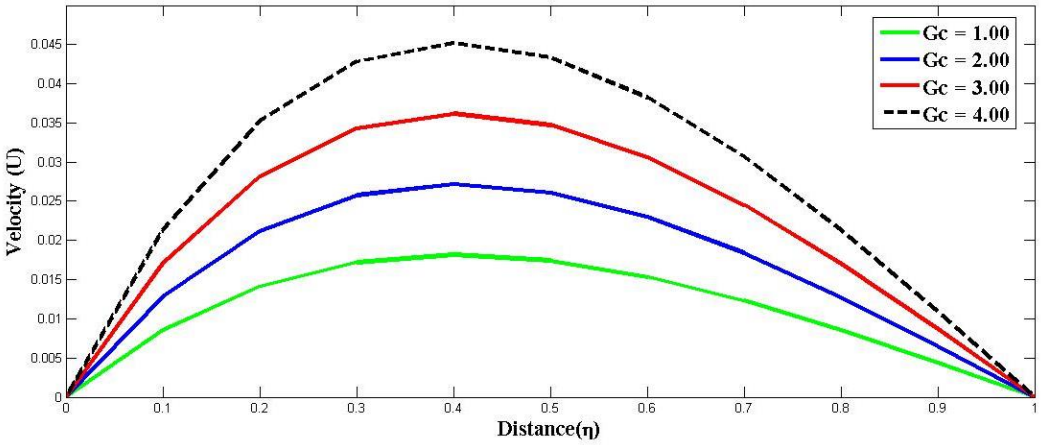

Figure 7: Velocity profile variations for Gc.

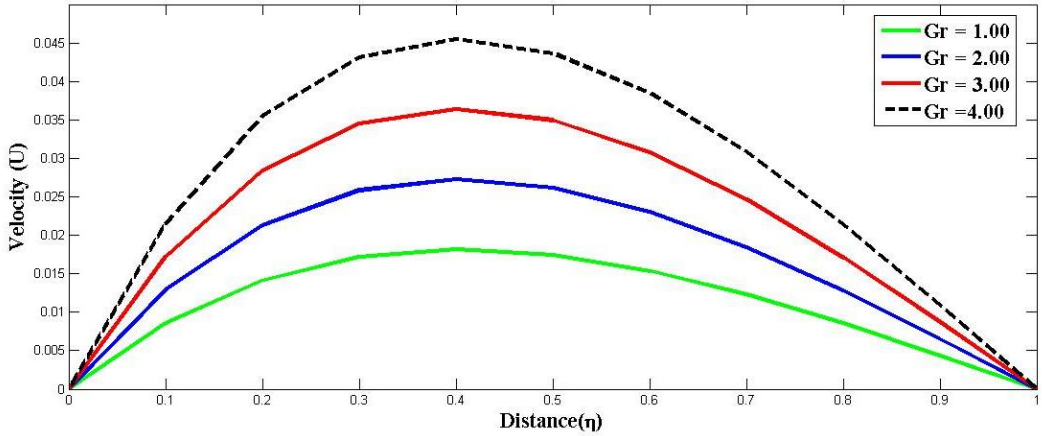

Figure 8: Velocity profile variations for Gm.

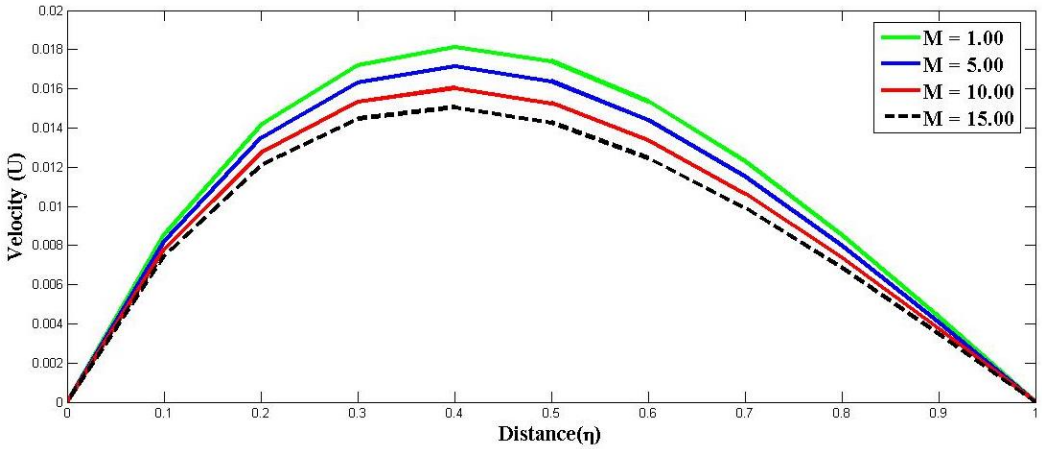

Figure 9: Velocity profile variations for M.

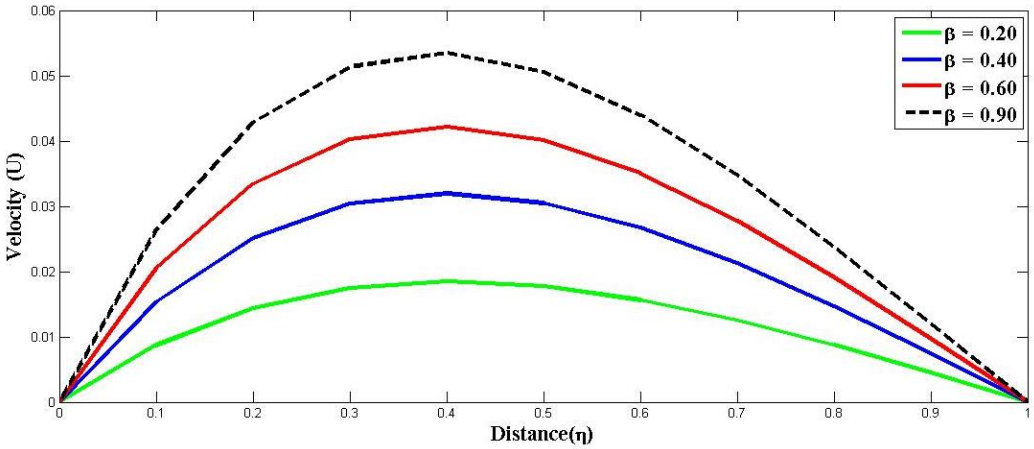

Figure 10: Velocity profile variations for β.

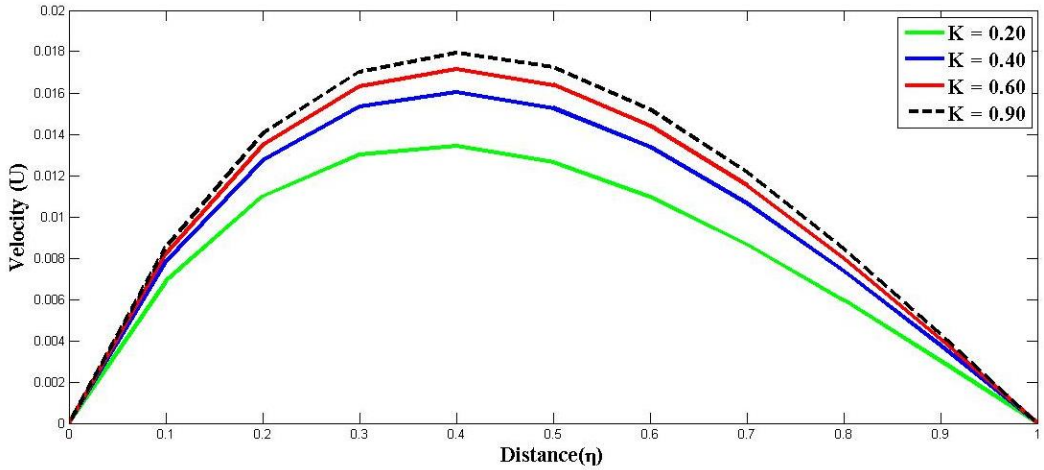

Figure 11: Velocity profile variations for K.

Illustration for Temperature Profile

Figure 12 illustrates the effect of suction on the thermal boundary layer. It is evident that the temperature of the fluid reduces as suction parameter is increased. The effect to Dufour is displayed in Figure 13. It is found that rise in the Dufour parameter causes the temperature to rise significantly while a reverse trend is observed as the Prandtl number increases as shown in Figure 14. With an increase in the heat sink parameter as shown in Figure 15, the temperature profile is noted to become steeper with a higher temperature at the surface. The reason for this is because, as the heat sink parameter increases, more heat energy is introduced in to the system causing the fluid temperature to be raised. Due to this additional internal heat generation, the thermal energy of the fluid, more particularly the region close to the surface where heat is generated, will be elevated which in turn increases the temperature profile. Because heat is now continuously being applied to the fluid, the thermal boundary layer grows thicker as the fluid is able to gain more energy and the temperature within the surface region is raised

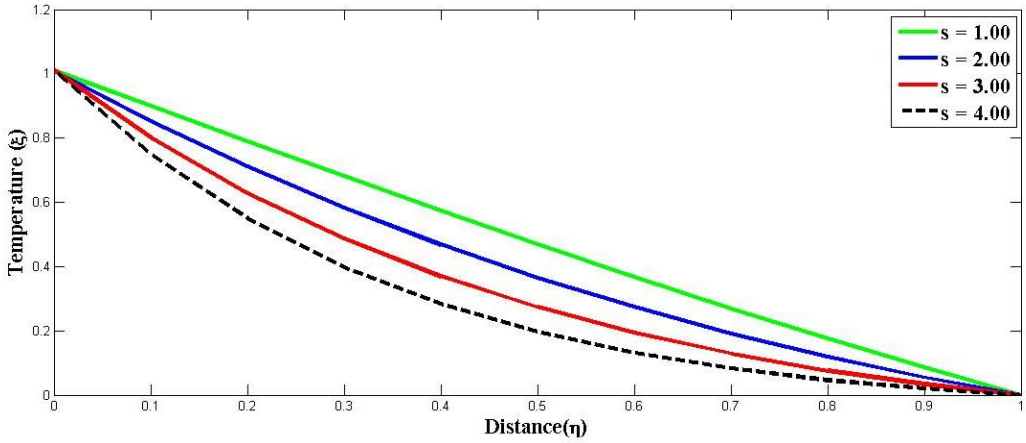

Figure 12: Temperature profile variations for s.

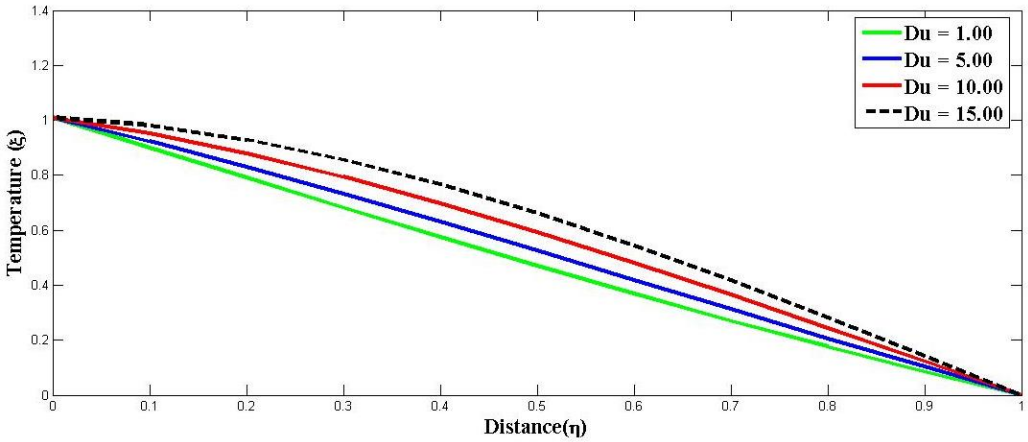

Figure 13: Temperature profile variations for Du.

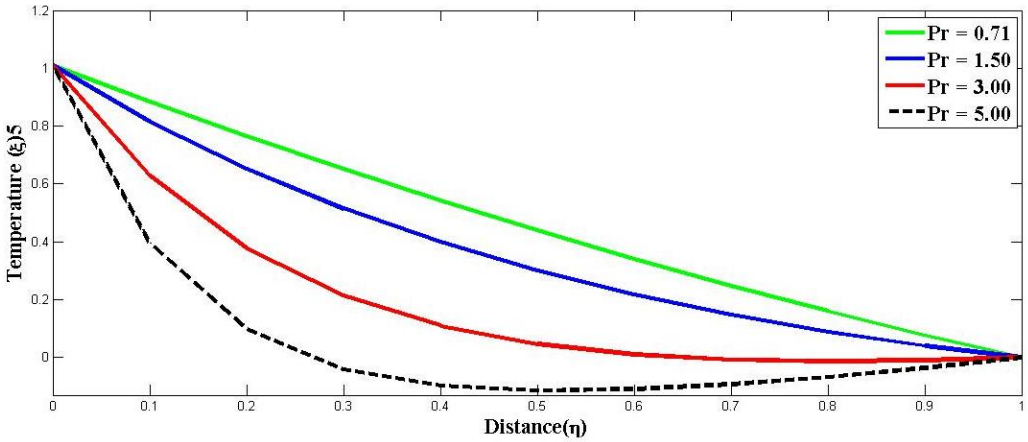

Figure 14: Temperature profile variations for Pr.

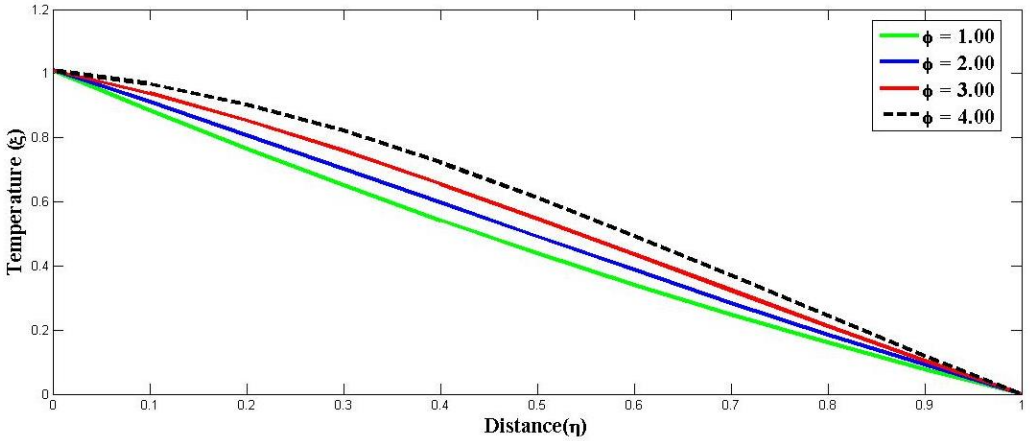

Figure 15: Temperature profile variations for φ_1.

Illustration for Concentration Profiles

Figures 16 and 17 show the effect of suction and chemical reaction, respectively, on the concentration profile. It is seen that the fluid's concentration falls as suction and chemical reaction parameters are increased. Figure 18 depicts the effect of Schmidt number on the concentration profile. As can be seen, an increase in Schmidt number results in a lesser concentration of the overall concentration profiles. Essentially, an increase in the Schmidt implies that mass diffusivity is relatively low compared to the momentum diffusivity. This means that the concentration boundary layer which indicates the mass or concentration of a species in a fluid Gets thick. Thicker concentration of boundaries means that mass diffusion in regions of large target density is relatively slower in comparison to diffusion of species throughout the medium. This makes the change in concentration profile, with distance from the target wall, relatively steep. Hence, once a mass is concentrated at a boundary layer, diffusion in other areas of the solution is significantly less. Hence with increasing Schmidt number, the average concentration profile lowers while becoming more intense closer to the surface layer but further from the surface layer lowers the profile considerably due to being unable to diffuse across the boundary layer.

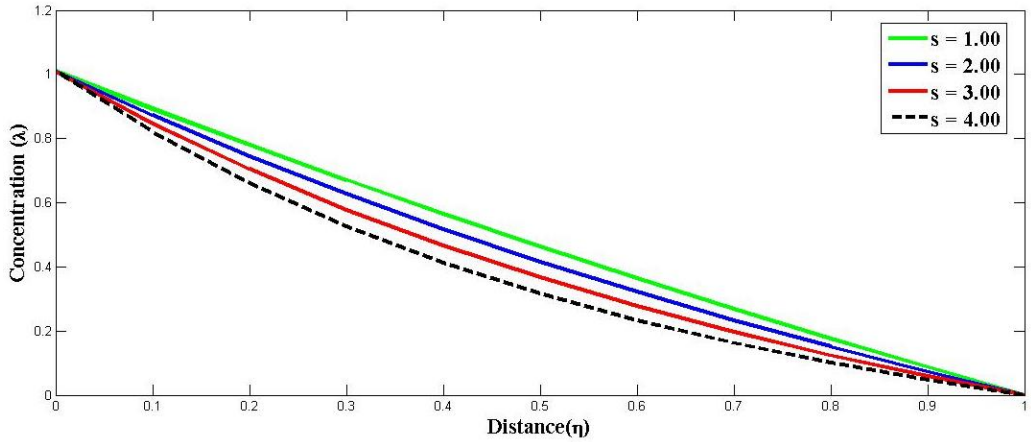

Figure 16: Concentration profile variations for s.

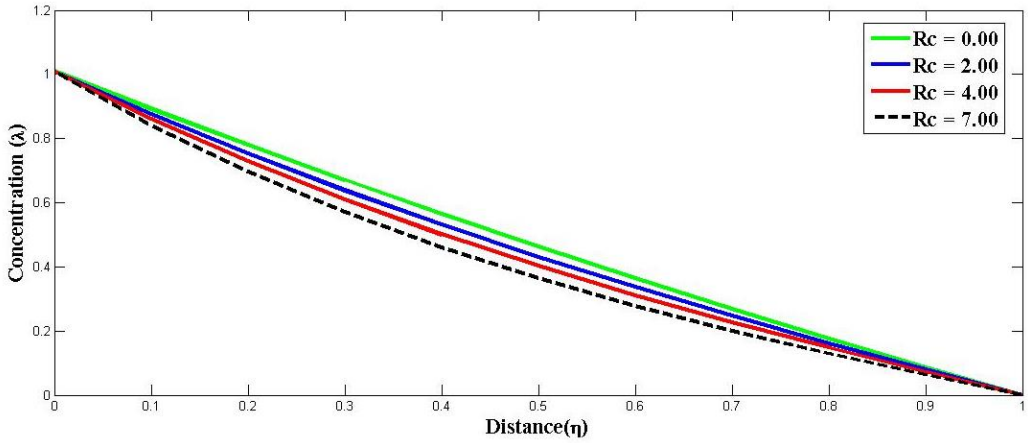

Figure 17: Concentration profile variations for Rc.

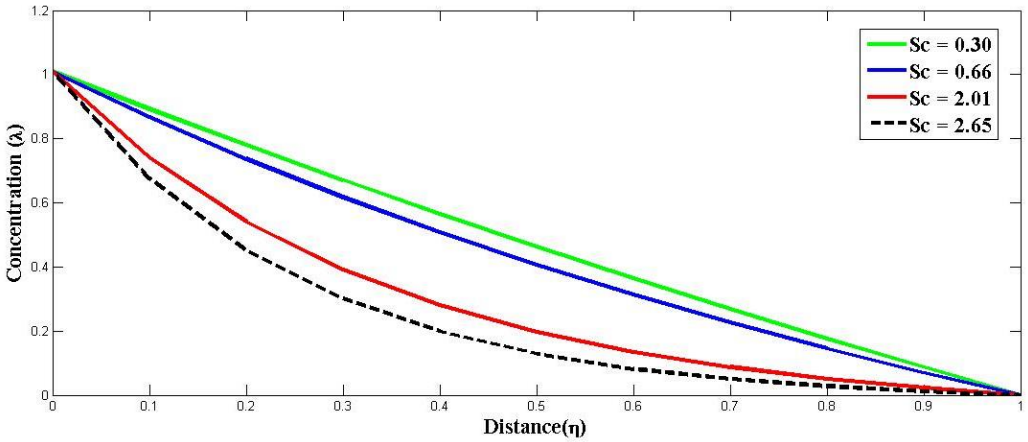

Figure 18: Concentration profile variations for Sc.

Concentration

This research looks at the physics of fluid flow, heat and mass transfer for Casson fluid flowing through a vertical channel incorporating Dufour and heat sink under some important varying physical parameters. The differential equations governing the phenomena were analytically solved by regular perturbation method and the findings were illustrated in graphs to show how these parameters affect the velocity, temperature and concentration profiles. The most important concluding remarks are summarised as follows:

i. An increase in the Casson parameter improves the velocity profile since fluids with low shear stress will not yield. In contrast, higher shear stresses will cause yielding, resulting in a steady and higher flow.
ii. Both the thermal and mass Grashof numbers enhance the velocity profile, indicating the influence of buoyancy forces driven by temperature and concentration gradients.
iii. The Prandtl number, chemical reaction and magnetic parameters was observed to have an adverse effect on the velocity profile. However, it was also noted that an increase in the porosity, and Dufour parameters improve the velocity profile suggesting that significance of these factors facilitate greater fluid movement.
iv. As the heat sink parameter increases, the velocity profile also increases, as the added thermal energy helps reduce the fluid's viscosity, thereby promoting fluid motion.

Conversely, this also expands the temperature profile due to continuous heating in the system.

v. Higher values of Schmidt numbers result in a reduction in the velocity profile due to an increase in mass diffusion resistance. Additionally, a rise in Schmidt numbers leads to a decrease in the concentration profile because mass diffusion is retarded.

Practical Relevance

This study could prove useful in areas such as: industrial heat management, geophysical fluid dynamics and chemical engineering processes. Examining features such as thermal and mass Grashof numbers, Dufour, and heat sink, have a potential in aiding the improvement of both heat and mass transfer in systems attached to channel flows, these include: cooling technologies, filtration systems, and energy storing systems. For instance, the results illustrate that the variation of heat sink parameters can be used to improve the thermal efficiency of devices such as: solar collectors and nuclear reactors. Moreover, the dependence of the velocity and temperature profiles on the magnitude of the magnetic parameter is important in the context of magnetohydrodynamic (MHD) pumps and flow control in electrically conducting fluids.

Future Directions

Further elaboration to this work could be done by applying more complicated boundary conditions such as: time varying heat flux or mixed convection to make the environment more realistic. This could potentially facilitate research on the behaviour of non-Newtonian fluids, which are often characterized by additional rheological attributes such as: viscoelastic and shear thickening, and broaden the model's applications. Computational simulations and three-dimensional modelling would enhance comprehension of the spatial impact and transient dynamics, warranting wider applicability in industrial and environmental systems.

References

Anwar, T., Kumam, P. & Watthayu, W. (2021). Unsteady MHD natural convection flow of Casson fluid incorporating thermal radiative flux and heat injection/suction mechanism under variable wall conditions. *Journal of scientific reports.* 11,4275. https://doi.org/10.1038/s41598-021-83691-2.

Babu, R.S., Venkateswarlu, S., VLakshmi, J.K. (2018). Effect of magnetic field and radiation on MHD heat and mass transfer of micropolar fluid over stretching sheet with Soret and Dufour effects. *International Journal of Applied Engineering Research.* 13(12), Pp: 10991–11000. http://www.ripublication.com

Dinesh, P. A., Gayathri, M. S., Suma, K. V., Shilpa, B. V., & Chandrashekhar, D. V. (2023). Soret effect on mixed convection of casson fluid flow in presence of porous media in a porous channel. *Journal of Mines, Metals and Fuels*, 2837-2847.

Falodun, B. O., & Ahamed, M. S. (2019). Soret and Dufour effects on unsteady Casson magneto-nanofluid flow over an inclined plate embedded in a porous medium. *World Journal of Engineering*, *16*(2), 260-274. https://doi.org/10.1108/WJE-04-2018-0144.

Gbadeyan, J. A., Oyekunle, T. L., Fasogbon, P. F., Abubakar, J. U. (2018). Soret and Dufour effects on heat and mass transfer in chemically reacting MHD flow through a wavy channel. *Journal of Taibah University for Science.* 12(5), Pp: 631–651. https://doi.org/10.1080/16583655.2018.1492221.

Grosan, T., & Pop, I. (2007). Thermal radiation effect on fully developed mixed convection flow in a vertical channel. *Technische Mechanik-European Journal of Engineering Mechanics*, *27*(1), 37-47.

Ismail, Z., Hashim, M. R., Mohamad, A. Q., Shafie, S., Vieru, D., & Sibaroni, Y. (2025). Analytical solution of brinkman type fluid in vertical channel with suction and injection effects: Water filtration application. *Journal of Advanced Research in Fluid Mechanics and Thermal Sciences,* 130(1), 1-10. https://doi.org/10.37934/arfmts.130.1.110

Israel-Cookey, C., Davies, O. A., & Ngeri, A. P. (2023). Magnetohydrodynamic forced convection and heat transfer of a Casson fluid flow in an anisotropic porous channel with isoflux boundaries. *World Journal of Advanced Research and Reviews, 18*(03), 1332-1347. https://doi.org/10.30574/wjarr.2023.18.3.1214

Kumam, P., Shah, Z., Watthayu, W., & Anwar, T. (2021). Radiative MHD unsteady Casson fluid flow with heat source/sink through a vertical channel suspended in porous medium subject to generalized boundary conditions. *Physica Scripta, 96*(7), 075213. https://doi.org/10.1088/1402-4896/abe14a

Kumar, S. and Singh, A. (2023). Application of the Casson fluid model in food processing: ketchup and toothpaste rheology. *Food Science & Nutrition.* 11(4). 2351-2360. DOI: https://doi.org/10.1002/fsn3.2877.

Kumar, V. V., Shekar, M. R., & Bejawada, S. G. (2025). Thermo diffusion and radiation impacts on heat and mass transfer Casson fluid flow with porous medium with chemical reaction. *Chemical Thermodynamics and Thermal Analysis*, 18. https://doi.org/10.1016/j.ctta.2025.100192

Nur, A. M. M., Nur, A. S., Noor, A. N. M. Z., Dimas, A. M., Amirah, S., & Izzati, K. K. (2024). Significant effect of radiation on combined convection vertical channel with internal heat generation and boundary conditions of a third kind. *Journal of Advanced Research in Numerical Heat Transfer*, *18*(1), 14–29. https://doi.org/10.37934/arnht.18.1.1429

Ojemeri, G. and Hamza, M. M. (2022). Heat transfer analysis of arrhenius-controlled free convective hydromagnetic flow with heat generation/absorption effect in a micro-channel. *Alexandria Engineering Journal.* 61, pp. 12797-12811. DOI: https://doi.org/10.1016j.aej.2022.06.58.

Ojemeri, G., Shuiabu, A., Abubakar, A. Y., Usman, I. O. and Ahmad, I. S. (2025).Dynamics of viscous Casson fluid on combined convection flow with exothermic chemical reaction in an upstanding tube. *Continental Journal of Applied Sciences*. 20 (1), 61 – 79. https://doi.org/10.5281/zenodo.14925803.

Oni, M. O. and Jha, B. K. (2019). Heat generation/absorption effect on natural convection flow in a vertical annulus with time-periodic boundary conditions. *Journal of Aircraft and Spacecraft technology*. 3(1), 183-196. https://doi.org/10.3844/jastsp.2019.183.196

Prakash, J., Selvaraj, A., Ragupathi, P., Al-Mdallal, Q. M., & Saranya, S. (2025). Thermal and radiative effects on unsteady MHD flow of Casson fluid past a rotating porous medium with variable mass diffusion. *Case Studies in Thermal Engineering*, https://doi.org/10.1016/j.csite.2025.105865.

Qiang, X., Siddique, I., Sadiq, K., and Shah, N. A. (2020). Double diffusive MHD convective flows of a viscous fluid under influence of the inclined magnetic field, source/sink and chemical reaction. *Alexandria Engineering Journal*. 59,4172. https://doi.org/10.1016/j.aej.2020.07.023.

Ramesh, N. L., Dinesh, P. A., & Shilpa, B. V. (2023). Effect of diffusion-thermal on mixed convective Casson fluid flow in a porous channel. *Journal of Mines, Metals and Fuels*, 1526-1536.

Shankar, G., & Sheri, S. R. (2025). Unsteady MHD Casson fluid flow past a vertical plate in the presence of viscid dissipation and Dufour effects. *Multidiscipline Modeling in Materials and Structures, 21*(2), 362-386. https://doi.org/10.1108/MMMS-07-2024-0191

Sharma, K, and Bhaskar, K. (2020) Influence of Soret and Dufour on three dimensional MHD flow considering thermal radiation and chemical reaction. *International Journal of Applied Computer Mathematics.* 6(1):3.

Uwanta, I. J. and Hamza, M. M. (2014). Unsteady flow of reactive viscous, heat generating/absorbing fluid with Soret and variable thermal conductivity. *International Journal of Chemical Engineering*. https://doi.org/10.1155/2014/291857.

Vinod, Y., Nagappanavar, S. N., Raghunatha, K. R., & Sangamesh. (2024b). Dufour and Soret effects on double diffusive Casson fluid flow with the influence of internal heat source. *Journal of Umm Al-Qura University for Applied Sciences*, 1-11. http://dx.doi.org/10.1007/s43994-024-00133-1

Vinod, Y., Suma N. N., Raghunatha, K. R. and Sangamesh (2024a). Dufour and Soret effects on double diffusive Casson fluid flow with the influence of internal heat source. *Journal of Umm Al-Qura University for Applied Sciences*. Pp 1-5. https://doi.org/10.1007/s43994-024-00133-1.

Xu, H., & Pop, I. (2012). Fully developed mixed convection flow in a vertical channel filled with nanofluids. *International Communications in Heat and Mass Transfer, 39*(8), 1086-1092.

Appendix

$$a_1 = \sqrt{\frac{(ScS)^2 + 4(ScKc)}{4}}$$

$$a_2 = \sqrt{\frac{(ScS)^2 + 4(iwSc + ScKc)}{4}}$$

$$n_2 = \frac{ScS}{2} + a_1$$

$$n_4 = \frac{ScS}{2} + a_2$$

$$A_1 = 1 - A_2$$

$$A_2 = \frac{-e^{n_1}}{\left(e^{-n_2} - e^{n_1}\right)}$$

$$A_3 = 1 - A_4$$

$$A_4 = \frac{-e^{n_3}}{\left(e^{-n_4} - e^{n_3}\right)}$$

$$\lambda_0(\eta) = A_1 e^{n_1\eta} + A_2 e^{-n_2\eta},$$

$$\lambda_1(\eta) = A_3 e^{n_3\eta} + A_4 e^{-n_4\eta}$$

$$a_3 = \sqrt{\frac{(\mathrm{Pr}S)^2 - 4(\mathrm{Pr}\varphi_1)}{4}}$$

$$a_4 = \sqrt{\frac{(\mathrm{Pr}S)^2 - 4(\mathrm{Pr}\varphi_1 + iw\mathrm{Pr})}{4}}$$

$$n_6 = \frac{\mathrm{Pr}S}{2} + a_3$$

$$n_8 = \frac{\mathrm{Pr}S}{2} + a_4$$

$$A_5 = 1 - A_6 - A_7 - A_8$$

$$A_6 = \frac{A_7(e^{n_5} - e^{n_1}) - A_8(e^{n_5} - e^{-n_2}) - e^{n_5}}{\left(e^{-n_6} - e^{n_5}\right)}$$

$$A_7 = \frac{-\Pr Drn_1^2 A_1}{n_1^2 + \Pr Sn_1 + \Pr \varphi_1}$$

$$A_8 = \frac{-\Pr Drn_2^2 A_2}{n_2^2 + \Pr Sn_2 + \Pr \varphi_1}$$

$$A_9 = 1 - A_{10} - A_{11} - A_{12}$$

$$A_{10} = \frac{A_{11}(e^{n_7} - e^{n_3}) - A_{12}(e^{n_7} - e^{-n_4}) - e^{n_7}}{\left(e^{-n_8} - e^{n_7}\right)}$$

$$A_{11} = \frac{-\Pr Drn_3^2 A_3}{n_3^2 + \Pr Sn_3 + (\Pr \varphi_1 - iw\Pr)}$$

$$A_{12} = \frac{-\Pr Drn_4^2 A_4}{n_4^2 + \Pr Sn_4 + (\Pr \varphi_1 - iw\Pr)}$$

$$\xi_0(\eta) = A_5 e^{n_5\eta} + A_6 e^{-n_6\eta} + A_7 e^{n_1\eta} + A_8 e^{-n_2\eta}$$

$$\xi_1(\eta) = A_9 e^{n_7\eta} + A_{10} e^{-n_8\eta} + A_{11} e^{n_3\eta} + A_{12} e^{-n_4\eta}$$

$$\gamma = \left(\frac{1}{\beta} + 1\right)$$

$$a_5 = \sqrt{\frac{\left(\frac{S}{\gamma}\right)^2 + 4\left(\frac{M}{\lambda} + \frac{1}{K}\right)}{4}}$$

$$a_6 = \sqrt{\frac{\left(\frac{S}{\lambda}\right)^2 + 4\left(\left(\frac{M}{\lambda} + \frac{1}{K}\right) + \frac{iw}{\gamma}\right)}{4}}$$

$$n_{10} = \frac{\frac{S}{\gamma}}{2} + a_5$$

$$n_{12} = \frac{\frac{S}{\gamma}}{2} + a_6$$

$$A_{13} = -A_{14} - A_{15} - A_{16} - A_{17} - A_{18} - A_{19} - A_{20}$$

$$A_{14} = \frac{A_{15}(e^{n_9} - e^{n_5}) + A_{16}(e^{n_9} - e^{-n_6}) + A_{17}(e^{n_9} - e^{n_1}) + A_{18}(e^{n_9} - e^{-n_2}) + A_{19}(e^{n_9} - e^{n_1}) + A_{16}(e^{n_9} - e^{-n_6})}{\left(e^{-n_8} - e^{n_7}\right)}$$

$$A_{15} = \frac{-GrA_5}{\gamma\left(n_5^2 + \frac{S}{\gamma}n_5 - \left(\frac{M}{\gamma} + \frac{1}{K}\right)\right)}$$

$$A_{16} = \frac{-GrA_6}{\gamma\left(n_6^2 - \frac{S}{\gamma}n_6 - \left(\frac{M}{\gamma} + \frac{1}{K}\right)\right)}$$

$$A_{17}=\frac{-GrA_7}{\gamma\left(n_1^2+\frac{S}{\gamma}n_1-\left(\frac{M}{\gamma}+\frac{1}{K}\right)\right)}$$

$$A_{18}=\frac{-GrA_8}{\gamma\left(n_2^2-\frac{S}{\gamma}n_2-\left(\frac{M}{\gamma}+\frac{1}{K}\right)\right)}$$

$$A_{19}=\frac{-GmA_1}{\gamma\left(n_1^2+\frac{S}{\gamma}n_1-\left(\frac{M}{\gamma}+\frac{1}{K}\right)\right)}$$

$$A_{20}=\frac{-GmA_2}{\gamma\left(n_2^2-\frac{S}{\gamma}n_2-\left(\frac{M}{\gamma}+\frac{1}{K}\right)\right)}$$

$$A_{21}=-A_{22}-A_{23}-A_{24}-A_{25}-A_{26}-A_{27}-A_{28}$$

$$A_{22}=\frac{A_{23}(e^{n_{11}}-e^{n_7})+A_{24}(e^{n_{11}}-e^{-n_8})+A_{25}(e^{n_{11}}-e^{n_3})+A_{26}(e^{n_{11}}-e^{-n_4})+A_{27}(e^{n_{11}}-e^{n_3})+A_{28}(e^{n_{11}}-e^{-n_4})}{\left(e^{-n_{12}}-e^{n_{11}}\right)}$$

$$A_{23}=\frac{-GrA_9}{\gamma\left(n_7^2+\frac{S}{\gamma}n_7-\left(\left(\frac{M}{\gamma}+\frac{1}{K}\right)+\frac{iw}{\gamma}\right)\right)}$$

$$A_{24}=\frac{-GrA_{10}}{\gamma\left(n_8^2-\frac{S}{\gamma}n_8-\left(\left(\frac{M}{\gamma}+\frac{1}{K}\right)+\frac{iw}{\gamma}\right)\right)}$$

$$A_{25}=\frac{-GrA_{11}}{\gamma\left(n_3^2+\frac{S}{\gamma}n_3-\left(\left(\frac{M}{\gamma}+\frac{1}{K}\right)+\frac{iw}{\gamma}\right)\right)}$$

$$A_{26}=\frac{-GrA_{12}}{\gamma\left(n_4^2-\frac{S}{\gamma}n_4-\left(\left(\frac{M}{\gamma}+\frac{1}{K}\right)+\frac{iw}{\gamma}\right)\right)}$$

$$A_{27}=\frac{-GmA_3}{\gamma\left(n_3^2+\frac{S}{\gamma}n_3-\left(\left(\frac{M}{\gamma}+\frac{1}{K}\right)+\frac{iw}{\gamma}\right)\right)}$$

$$A_{28}=\frac{-GmA_4}{\gamma\left(n_4^2-\frac{S}{\gamma}n_4-\left(\left(\frac{M}{\gamma}+\frac{1}{K}\right)+\frac{iw}{\gamma}\right)\right)}$$

$$U_0(\eta)=A_{13}e^{n_9\eta}+A_{14}e^{-n_{10}\eta}+A_{15}e^{n_5\eta}+A_{16}e^{-n_6\eta}+A_{17}e^{n_1\eta}+A_{18}e^{-n_2\eta}+A_{19}e^{n_1\eta}+A_{20}e^{-n_2\eta}$$

$$U_1(\eta)=A_{21}e^{n_{11}\eta}+A_{22}e^{-n_{12}\eta}+A_{23}e^{n_7\eta}+A_{24}e^{-n_8\eta}+A_{25}e^{n_3\eta}+A_{26}e^{-n_4\eta}+A_{27}e^{n_3\eta}+A_{28}e^{-n_4\eta}$$